Published for SISSA by Springer

Received: March 7, 2025
Revised: May 6, 2025
Accepted: June 24, 2025
Published: July 18, 2025

Double Higgs production in vector boson fusion at NLO QCD in HEFT

Jens Braun,[a] **Pia Bredt**,[b] **Gudrun Heinrich**[a] **and Marius Höfer**[a]

[a] *Institute for Theoretical Physics, Karlsruhe Institute of Technology (KIT), Wolfgang-Gaede-Str. 1, 76131 Karlsruhe, Germany*
[b] *Department of Physics, University of Siegen, Walter-Flex-Straße 3, 57068 Siegen, Germany*

E-mail: j.braun@kit.edu, pia.bredt@uni-siegen.de, gudrun.heinrich@kit.edu, marius.hoefer@kit.edu

Abstract: We present the next-to-leading order QCD corrections to Higgs boson pair production in vector boson fusion, including the leading operators in the framework of Higgs Effective Field Theory (HEFT). The corresponding calculation is based on an automated interface between the Monte Carlo event generator Whizard and the one-loop amplitude generator GoSam. The QCD corrections also include non-factorising diagrams and diagrams of Higgs-Strahlung type, thus going beyond the structure function approach. We find that some constellations of anomalous couplings, while being well within the current experimental constraints, can have a significant impact on the shape of typical observables for this process.

Keywords: Anomalous Higgs Couplings, Higgs Production, Higher-Order Perturbative Calculations

ArXiv ePrint: 2502.09132

https://doi.org/10.1007/JHEP07(2025)209

JHEP07(2025)209

Contents

JHEP07(2025)209

1 Introduction

The production of two Higgs bosons ranks among the most important processes at the Large Hadron Collider (LHC), in particular in view of its High-Luminosity phase, as well as at prospective future colliders, because it allows us to shed more light on the trilinear Higgs-boson self-coupling, and thus on the Higgs potential. While Higgs boson pair production through gluon fusion has the largest cross section among all di-Higgs production modes at the LHC, the production of a Higgs boson pair through vector boson fusion (VBF) has several appealing features: experimentally motivated, as the two jets originating from the VBF process allow to tag on a distinct signature, and theoretically motivated, as the coupling of Higgs bosons to vector bosons is intimately linked to unitarity and therefore small deviations in the couplings can have large effects.

The experimental collaborations already have put combined constraints on Higgs couplings to vector bosons and to itself, see refs. [1–4] for recent results.

In the Standard Model (SM), QCD corrections to Higgs boson pair production through VBF have been calculated to very high order. The next-to-leading order (NLO) QCD corrections were first calculated in refs. [5–7] and are available in the codes `VBFNLO` [8, 9] and `MadGraph5_aMC@NLO` [10]. Differential next-to-next-to-leading order (NNLO) QCD corrections in the in the so-called *structure function approximation*, where the process is treated as two factorising DIS-like topologies, have been calculated in refs. [11, 12], the total cross section is also available at next-to-next-to-next-to-leading order (N3LO) [13]. In ref. [14], the NNLO QCD corrections are combined with NLO electroweak (EW) corrections. The non-factorisable corrections appearing at NNLO, which can reach the 2% level for large jet

transverse momenta, have been calculated in the eikonal approximation in ref. [15] and have been implemented in the code `proVBFHH` [16].

Opportunities to use the distinctive features of VBF Higgs pair production versus gluon fusion have been studied in refs. [17, 18], a strategy to extract the $hhVV$ quartic coupling has been proposed in ref. [19].

The importance of the VBF process for di-Higgs production within Effective Field Theories (EFT) to constrain anomalous Higgs couplings has been pointed out already some time ago [20–24] and has been studied under the aspect of distinguishing linear from non-linear realisations of the Higgs sector [25–29]. The latter are also known under the name *Electroweak Chiral Lagrangian* or *Higgs Effective Field Theory*[1] *(HEFT)* [30–38].

The publicly available Monte Carlo programs beyond LO for this process [6, 9, 14, 16, 39] so far either did not include anomalous couplings within an EFT framework, or did not include the full NLO QCD corrections without approximations. With this paper we close this gap, presenting results that include the leading EFT operators within HEFT as well as the full NLO QCD corrections, including also the diagrams of Higgs-Strahlung type leading to the same $hhjj$ final state. The code is based on a new version of the one-loop amplitude generator GoSam [40–42] combined with the Monte Carlo event generator Whizard [43, 44] through the BLHA interface [45, 46], using a model file in Universal Feynman Output (UFO) format [47, 48]. The code also allows the combination with a parton shower, which is however not studied in this work.

The paper is organised as follows. In section 2, we discuss the process and the contributions of the leading HEFT operators. In section 3 we describe our implementation, before we discuss the results for the total and differential cross sections in section 4 and conclude.

2 VBF in Higgs Effective Field Theory

2.1 Effective Lagrangian of Higgs Effective Field Theory

Under the assumption that the energy scale of New Physics resides well above the electroweak scale of the SM, a parametrisation of beyond SM physics in terms of an EFT is well justified. Two such theories are commonly used in that context, the Standard Model Effective Field Theory (SMEFT) [49–52] and the Higgs Effective Field Theory (HEFT) [30–38]. The former organises the power counting of its effective operators in terms of their canonical mass dimension and is valid under the assumption that the otherwise unknown UV physics is weakly coupled [53–55]. HEFT on the other hand is suited also as an EFT description of UV theories with strong coupling in the Higgs sector, like for example composite Higgs models. As a consequence the Higgs field is treated independently from the Goldstone bosons of electroweak symmetry breaking, and the power counting is organised in the chiral dimension d_χ, which is zero for bosons and one for each weak coupling, derivative and fermion bilinear [56]:

$$d_\chi\left(X_\mu, S\right) = 0\,, \qquad d_\chi\left(\kappa, \partial, \bar{\psi}\psi\right) = 1\,. \tag{2.1}$$

[1] Which is not to be confused with the heavy top-quark limit of the SM, which is also sometimes referred to as HEFT.

JHEP07(2025)209

Here X_μ and S represent generic gauge and scalar fields, respectively, and κ can be any gauge or Yukawa coupling.[2] For any given operator the chiral dimension directly corresponds to the operator's loop order L, $d_\chi = 2L + 2$. HEFT is particularly suited when one expects new physics effects to show dominantly in anomalous Higgs couplings. The leading order (LO) HEFT Lagrangian collects all terms of chiral dimension $d_\chi = 2$ and is given by [38]

$$\begin{aligned}\mathcal{L}_2 = &-\frac{1}{4}G^a_{\mu\nu}G^{a\mu\nu} - \frac{1}{2}\langle W_{\mu\nu}W^{\mu\nu}\rangle - \frac{1}{4}B_{\mu\nu}B^{\mu\nu} \\ &+ \frac{v^2}{2}\partial_\mu\eta\,\partial^\mu\eta - V(\eta) + \frac{v^2}{4}\left\langle (D_\mu U)^\dagger (D^\mu U)\right\rangle F(\eta) \\ &+ \bar{\psi} i\not{D}\psi - \bar{\psi}\left(U\mathcal{M}(\eta)P_R + \mathcal{M}^\dagger(\eta)U^\dagger P_L\right)\psi\,,\end{aligned} \tag{2.2}$$

with the $\mathrm{SU}(3)_C$, $\mathrm{SU}(2)_L$ and $\mathrm{U}(1)_Y$ field strengths $G^a_{\mu\nu}$, $W^\alpha_{\mu\nu}$ and $B_{\mu\nu}$, and $\eta = h/v$, with h being the Higgs singlet field and v the scale of electroweak symmetry breaking. Angled brackets $\langle \dots \rangle$ denote a trace over $\mathrm{SU}(2)_L$ group indices. For the sake of a compact notation the fermions are grouped into $\psi = (u, d, \nu, e)^T$, where each entry is a Dirac spinor and has to be understood as a vector in generation space. P_R and P_L are the usual right and left-handed projectors, such that $P_L\psi = (u_L, d_L, \nu_L, e_L)^T \equiv (Q_L, L_L)^T$ and $P_R\psi = (u_R, d_R, 0, e_R)^T$, with Q_L, L_L and u_R, d_R, e_R the usual $\mathrm{SU}(2)_L$ doublet and singlet fields, respectively. The fermions' covariant derivative is then given by

$$D_\mu\psi = \left(\partial_\mu + ig_s G_\mu + igW_\mu P_L + ig'B_\mu(Y_L P_L + Y_R P_R)\right)\psi\,, \tag{2.3}$$

where $G_\mu = G^a_\mu T^a$, $W_\mu = W^\alpha_\mu t^\alpha$, with T^a and t^α denoting the generators of $\mathrm{SU}(3)_C$ and $\mathrm{SU}(2)_L$, respectively. Their normalisation is given by $\mathrm{Tr}(T^a T^b) = \delta^{ab}/2$ and $\langle t^\alpha t^\beta\rangle = \delta^{\alpha\beta}/2$. The hypercharges are $Y_L = \mathrm{diag}(1/6, 1/6, -1/2, -1/2)$ and $Y_R = \mathrm{diag}(2/3, -1/3, 0, -1)$.

In HEFT the Higgs potential $V(\eta)$ is a Maclaurin series in η,

$$V(\eta) = v^4 \sum_{n=2}^{\infty} V_n \eta^n\,, \tag{2.4}$$

generating self-interactions with an arbitrary number of Higgs bosons. The Goldstone sector of the electroweak symmetry is realised by means of the object $U = \exp(2i\varphi/v)$, where $\varphi = \varphi^\alpha t^\alpha$ are the Goldstone bosons. The covariant derivative of U induces the interaction between the electroweak gauge bosons and the Goldstones,

$$D_\mu U = \partial_\mu U + igW_\mu U - ig'B_\mu U t^3\,. \tag{2.5}$$

Here g and g' are the gauge couplings of $\mathrm{SU}(2)_L$ and $\mathrm{U}(1)_Y$, respectively. The so-called Flare function

$$F(\eta) = 1 + \sum_{n=1}^{\infty} F_n \eta^n \tag{2.6}$$

generates interactions between electroweak gauge and Goldstone bosons and an arbitrary number of Higgs fields.

[2]The coefficients appearing in the functions $V(\eta)$, $F(\eta)$ and $\mathcal{M}(\eta)$ defined below are assumed to be radiatively generated and thus contain implicit factors of κ. See [56] for details.

JHEP07(2025)209

The kinetic term of quarks and leptons is as in the SM, while the extended Yukawa sector of HEFT is expressed in terms of the generalised, block diagonal mass matrix $\mathcal{M} = \text{diag}\,(\mathcal{M}_u, \mathcal{M}_d, \mathcal{M}_\nu, \mathcal{M}_e)$, where the $\mathcal{M}_f(\eta)$ are functions of the Higgs field, again inducing interactions with an arbitrary number of Higgs bosons,

$$\mathcal{M}_f(\eta) = m_f + \sum_{n=1}^{\infty} \mathcal{M}_{f,n}\eta^n \,. \tag{2.7}$$

We note that the LO HEFT Lagrangian (2.2) does not generate anomalous couplings without at least one Higgs field. In particular, the gauge-fermion interactions remain SM-like, and there are no purely fermionic operators at this order. The exact SM Lagrangian can be recovered from (2.2) by setting

$$\begin{aligned} V_2 = V_3 = m_h^2/2v^2\,, \qquad & V_4 = m_h^2/8v^2\,, \qquad & V_{n\geq 5} = 0\,, \\ F_1 = 2\,, \qquad & F_2 = 1\,, \qquad & F_{n\geq 3} = 0\,, \\ \mathcal{M}_{f,1} = m_f\,, \qquad & \mathcal{M}_{f,n\geq 2} = 0\,. \end{aligned}$$

The LO HEFT Lagrangian (2.2) is not renormalisable in the classical sense, that is, not all UV divergences appearing in loop amplitudes constructed from $\mathcal{L}_2$ can be absorbed by renormalising its parameters. However, the renormalisation can be carried out order by order in the loop-, or equivalently chiral-dimension expansion. At the one-loop order, for example, operators with chiral dimension $d_\chi = 4$ are required to cancel all UV-divergences coming from $\mathcal{L}_2$. Those operators are collected in $\mathcal{L}_4$ and can be found in [38, 57, 58]. At $d_\chi = 4$ we encounter modified fermion-gauge interactions and pure fermionic operators that were absent in $\mathcal{L}_2$. The complete one-loop renormalisation in HEFT has been studied in [59–61].

We remark that one can in fact construct another contribution at chiral dimension $d_\chi = 2$, given by the operator

$$\mathcal{O}_{\beta_1} \sim v^2 \left\langle U^\dagger D_\mu U t^3 \right\rangle^2 \left(1 + \sum_{n=1}^{\infty} F_{\beta_1,n}\eta^n\right) , \tag{2.8}$$

with $\mathcal{O}(1)$ coefficients $F_{\beta_1,n}$. However, this operator violates the custodial symmetry and generates a tree level contribution to the electroweak T-parameter [62]. In the SM the custodial symmetry is an approximate symmetry which becomes exact in the limit of vanishing hypercharge and when the Yukawa couplings of isospin partners are equal, that is, $Y_u = Y_d$, and equivalently in the lepton sector. We then have $T = 0$. Non-vanishing hypercharge and differences between Yukawa couplings of isospin partners affect the T-parameter, but only at the one-loop order and beyond. $T = 0$ still holds at tree-level and deviations from this result due to radiative corrections are small. This is in line with the experimental bounds on the T-parameter [63], which also indicate that the contribution from $\mathcal{O}_{\beta_1}$ must be suppressed. Therefore, it is customary to treat the operator as loop suppressed and assign it to $\mathcal{L}_4$.

2.2 Effective Lagrangian for Higgs Pair Production in VBF

In practical applications it is sufficient to consider only a subset of all effective operators appearing in the HEFT Lagrangian. Focusing on Higgs boson pair production in VBF, and

JHEP07(2025)209

assuming that the coupling of the Higgs boson to light quarks is not drastically enhanced compared to the SM, there are only three potentially anomalous interactions from $\mathcal{L}_2$, which can be parametrised as follows,

$$\mathcal{L}_{\text{eff}} \supset \left(2c_V\frac{h}{v} + c_{2V}\frac{h^2}{v^2}\right)\left(m_W^2 W_\mu^+ W^{-\mu} + \frac{1}{2}m_Z^2 Z_\mu Z^\mu\right) + c_\lambda \frac{m_h^2}{2v}h^3\,. \tag{2.9}$$

In terms of the parameters introduced in the previous section we have $c_V = F_1/2$, $c_{2V} = F_2$ and $c_\lambda = 2v^2V_3/m_h^2$. The normalisation of the c_i is chosen such that they all equal to one in the SM case. The fact that Z and $W^\pm$ share the same coupling is a consequence of the aforementioned conservation of the custodial symmetry.

We do not include any operators from $\mathcal{L}_4$ in our analysis, which we motivate as follows. In principle it is true that, when performing an NLO calculation, also operators with chiral dimension $d_\chi = 4$, i.e. one-loop order, have to be considered. Tree-level amplitudes with a single vertex insertion from $\mathcal{L}_4$ are of the same order as genuine one-loop amplitudes constructed from $\mathcal{L}_2$ vertices only. Here, however, we explicitly restrict ourselves to NLO in QCD. It follows that the one-loop corrections we encounter are $\mathcal{O}\left(g_s^2\right)$ relative to the Born diagrams, which are $\mathcal{O}\left(g_{ew}^4\right)$ for Higgs boson pair production in VBF.[3] It is therefore consistent to include only NLO HEFT operators contributing at the same power in the QCD coupling. Although the HEFT operators do not exhibit explicit powers in either the electroweak or strong coupling, one can still make a formal assignment based on the potential UV-origin of those operators. For example, each gauge field appearing in a given operator has to couple with the appropriate gauge coupling constant, which also holds for interactions with particles from the UV theory. Similarly, from power counting arguments it follows that each Higgs boson introduces a factor of $1/v \sim g_{ew}$. One can check that there are no operators from $\mathcal{L}_4$ with which we can construct tree topology diagrams matching the required configuration of external particles for Higgs pair production in VBF and the correct coupling powers for NLO QCD ($\mathcal{O}\left(g_{ew}^4 g_s^2\right)$) at the same time.

We should comment in particular on the operators from the classes X^2Uh and $XUhD^2$ in the nomenclature of [38], which couple a gauge field strength $X_{\mu\nu}$ to the electroweak Goldstones and an arbitrary number of Higgs bosons. From these operators we can get additional anomalous couplings between $W^\pm$, Z and h beyond the ones present in the LO effective Lagrangian (2.9), but also local interactions between Higgs bosons and photons and gluons. With the latter we can construct diagrams with ordinary VBF-topology (see figure 1 in the next section) with the electroweak vector bosons replaced by gluons. Those diagrams are one-loop suppressed because the anomalous gluon-Higgs couplings are loop-generated. This implies that they are of $\mathcal{O}\left(g_{ew}^2 g_s^4\right)$, since we can assign a power of $\mathcal{O}\left(g_{ew} g_s^2\right)$ ($\mathcal{O}\left(g_{ew}^2 g_s^2\right)$) to the ggh ($gghh$) couplings, motivated by the reasoning above. This does not match the coupling order of Higgs boson pair production in VBF and its NLO QCD corrections, so we do not include effective gluon-Higgs couplings in our analysis. Note that in the SM we can have a similar situation, with the gluons coupling to the Higgs boson via a top-quark loop: one-loop diagrams with the same external states as VBF can be constructed, but they are not considered as NLO QCD corrections to VBF.

[3] We use g_{ew} to count general electroweak couplings, i.e. both genuine gauge interactions and inverse powers of v appearing in Higgs-vertices.

JHEP07(2025)209

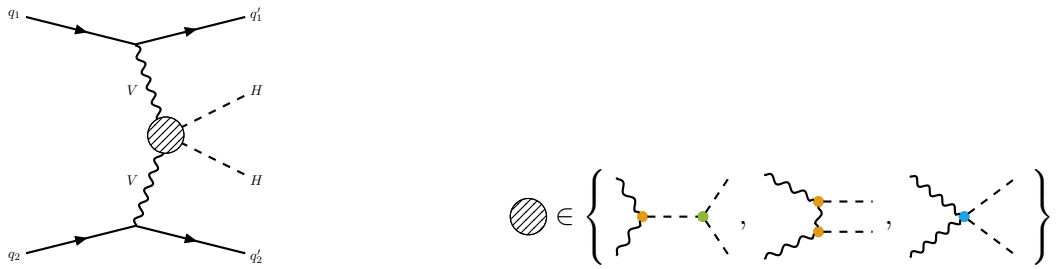

Figure 1. $pp \to hhjj$ at leading order. The shaded blob in the left diagram ((a)) can represent any of the sub-diagrams ((b)) on the right. We have massless quarks $q_i \in \{d, u, s, c, b\}$ and $V \in \{W^\pm, Z\}$. Crossings of s- and u-channel type are also allowed. See text for details.

A similar argument can be made for the $d_\chi = 4$ local interactions between the electroweak gauge bosons, including the photon, and the Higgs boson. They are all at least $\mathcal{O}\left(g_{ew}^3\right)$, leading to one-loop suppressed diagrams of $\mathcal{O}\left(g_{ew}^6\right)$. Thus those contributions are at the same level as NLO EW corrections and therefore discarded.

We conclude that the effective Lagrangian (2.9) is indeed sufficient to describe the leading anomalous EFT effects in Higgs boson pair production in VBF at NLO QCD. Hence there are no anomalous vertices with non-SM like Lorentz structures or field configurations and our setting coincides with that of the often used κ-framework [64, 65] with its coupling modifiers. Note that the situation changes when the NLO EW corrections are considered and additional operators from $\mathcal{L}_4$ become relevant. Those will introduce new vertex structures not present in the SM, which can not be covered within the κ-framework. See, for example, [66] for a more detailed comparison of HEFT with the κ-framework.

2.3 Higgs Boson Pair Production in VBF at NLO QCD

In this section we present all the contributions we considered for our calculation of Higgs boson pair production in VBF. Concretely, we define the process as electroweak Higgs boson pair production in proton-proton collisions in association with two light jets, i.e. $pp \to hhjj$ at $\mathcal{O}\left(\alpha_{ew}^4\right)$. We use g_{ew} or $\alpha_{ew} = g_{ew}^2/4\pi$ to keep track of any kind of electroweak couplings in the Feynman diagrams. The NLO QCD corrections then comprise all contributions of $\mathcal{O}\left(\alpha_s\right)$ relative to the Born level. We take the quarks of the first two generations and the bottom quark to be massless and neglect any couplings between them and the Higgs boson, both in the SM case and when including EFT effects. We do not consider top quarks as external states, and assume a diagonal CKM-matrix. The Born process is then given by the diagrams in figure 1. Since in our setup the Higgs boson does not couple to light quarks, it only interacts with the internal vector bosons $V = W^\pm, Z$. A Higgs boson pair can then be produced in three ways, depicted in figure 1(b): through a single hVV coupling with a subsequent splitting $h^* \to hh$ via the trilinear self-coupling, through two separate hVV couplings, or a single $hhVV$ coupling. As seen in the previous section, all three of the involved couplings can be anomalous, parametrised by c_λ, c_V and c_{2V}. In figure 1(b) they have been marked by green, orange and blue blobs, respectively.

JHEP07(2025)209

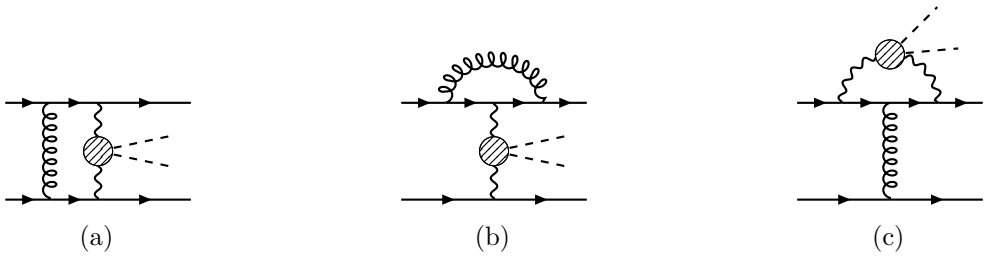

Figure 2. One-loop QCD corrections to $pp \to hhjj$. The shaded blob again represents any of the sub-diagrams in figure 1(b). s- and u-channel type crossings are allowed, too. See text for details.

We emphasise that, while the diagram in figure 1(a) is what is usually understood as a VBF topology, our process definition mentioned above allows for any of the two quarks to be crossed into the initial state. This means that besides the depicted t-channel-like topology we also include u- and s-channel-like diagrams. The latter, $q_i\bar{q}_j \to V^* \to q_k\bar{q}_l$ with V radiating two Higgs bosons, can be considered as a Higgs-strahlung topology instead. But since it matches the process definition in external states and coupling order, we will consider it in the following. Note, however, that diagrams of this kind are usually suppressed when VBF cuts are applied [14, 67].

At NLO QCD we have to consider both real and virtual (one-loop) corrections. The former can be constructed by attaching a single external gluon in any possible way to the quark lines in the Born process. The gluon can also be crossed into the initial state. For the virtual corrections on the other hand we have to consider all diagrams with an internal gluon added to the Born process. This gluon can be exchanged between the two separate quark lines as in figure 2(a), or be attached to a single quark line as in figure 2(b). The latter represent factorisable QCD corrections to the VBF process. In addition we can have diagrams as depicted in figure 2(c), where the two quark lines are connected through an internal gluon only and the two Higgs bosons are radiated from an electroweak-like loop. While this diagram does not have the usual VBF topology, it still has the correct external states and coupling order to be considered as part of the process.

Note that no additional anomalous couplings emerge at NLO QCD. Also, all anomalous couplings only appear in the sub-diagrams shown in figure 1(b), which do not receive any direct corrections at NLO QCD. The renormalisation of the amplitudes can be carried out as in the SM, no additional counterterms or modifications of counterterms are required.

3 NLO framework and setup

3.1 Tools

For the computation of cross sections and differential distributions we use an NLO framework which is composed of the event generator Whizard [43, 44] and the one-loop-provider GoSam [40, 41] — both operating for generic processes. For the analysis of the events and the generation of histograms we use Rivet [68, 69].

Whizard is a multi-purpose Monte Carlo program providing all parts of event generation for hadron and lepton collider processes; from the theoretical model to showered and

JHEP07(2025)209

hadronised events. It comes along with the intrinsic tree-level matrix element generator O'Mega [43] and the multi-channel phase space integrator Vamp [70], which is superseded by Vamp2 [71] with parallelisation capabilities based on the Message Passing Interface (MPI); this allows to run our simulation on multi-core architecture. We apply Whizard's NLO automated framework [72, 73] with real phase space construction and infrared subtraction following the FKS scheme [74, 75]. In principle, parton shower matched NLO event samples can be produced by the automated powheg matching [76] implementation in Whizard [77], which however is not considered for this work.

The amplitudes at the tree and one-loop level are computed by GoSam and passed to Whizard via its interface based on the Binoth Les Houches Accord (BLHA) standard [45, 46]. For their construction GoSam applies algebraic methods to generate analytical expressions for Feynman diagrams with the help of qgraf [78] and form [79, 80]. Subsequently, integral reduction is performed using the tool Ninja [81, 82] and the master integrals are evaluated with OneLoop [83]. The QCD UV renormalisation is done in an automated way in GoSam. The new version of GoSam [42] comes with improvements in the installation procedure and in speed; these features were also beneficial for the calculation presented here.

New code developments on the Whizard-GoSam interface allow the computation of NLO observables for user-defined hadron and lepton collider processes in the SM and beyond. For a consistent setup of both tools in view of New Physics models or Effective Field Theories, like HEFT or SMEFT, external model files are a key ingredient. All operators and vertices resulting from such theories can be summarised in files written in UFO format [47, 48], and thus are accessible by both tools via their separate UFO interfaces. The Whizard-GoSam interface has been extended to be able to cope with processes based on large classes of UFO model files.

Calculations with our setup can be done out-of-the-box providing a Whizard run file written in `Sindarin`, the steering language of this event generator, and an UFO model file in case the application of a theory beyond the SM is desired. We provide a repository[4] that contains the UFO model file and an example run file for the process considered here. Differential distributions at LO and NLO in the form of histograms, ultimately, can be produced by generating event samples with Whizard which are piped into a Rivet analysis in the next step.

3.2 Validation

We validated our Whizard-GoSam NLO framework by comparing several processes in the SM and in an EFT setup to the literature or to existing benchmarks. The setup using UFO model files has been extensively tested by comparing the results based on a SM UFO file to the case where the internal, well-validated, SM files have been used. As an example for an EFT setup, we carried out a comparison to the results of ref. [84] for the process $pp \to t\bar{t}H$ in SMEFT; the details of this comparison can be found in [85].

For the process considered here, we compared our setup at LO in the SM with `MadGraph5_aMC@NLO` and Whizard+OpenLoops, showing very good agreement. We also compared to `VBFNLO` and found agreement except in the tail of the $p_\perp^h$ distribution, which

[4] https://github.com/Jens-Braun/VBF_HH_HEFT.

JHEP07(2025)209

we attribute to the fact that VBFNLO uses the structure function approach. At NLO in the SM, a quantitative comparison at cross section level is difficult because the public tools that were available make approximations: if not the VBF approximation, then at least with regards to the treatment of the pentagon- and hexagon-integrals. Therefore we used OpenLoops [86, 87] to check our setup at amplitude level, and in combination with Whizard at the cross section level, yielding again good agreement. In particular, comparing GoSam and OpenLoops at amplitude level, we have evaluated 10^6 phase-space points for each, the Born amplitude squared, the real amplitude squared and the one-loop amplitude interfered with the Born amplitude. We found relative differences of $\mathcal{O}(10^{-15})$ for the Born- and real radiation amplitudes and of $\mathcal{O}(10^{-8})$ for the finite part of the virtual amplitude. More details about the validation can be found in ref. [88].

4 Phenomenological results

4.1 Input parameters

For the numerical evaluation of the process, we consider proton-proton collisions at the LHC with a centre-of-mass energy of $\sqrt{s} = 13.6\,\text{TeV}$. We use the PDF4LHC21_mc parton distribution function (PDF) set [89] obtained through LHAPDF6 [90] with the associated $\alpha_s(\mu)$. As the set of electroweak input parameters we use $\{\alpha, G_F, m_Z\}$, with the respective values of $\alpha^{-1}(m_Z) = 127.9$ and $G_F = 1.166\,37 \times 10^{-5}\,\text{GeV}^{-2}$. The masses and widths of the contributing particles, including the input parameter m_Z, are set to

$$\begin{aligned} m_Z &= 91.1876\,\text{GeV}, \quad \Gamma_Z = 2.4952\,\text{GeV}, \\ m_W(\alpha, m_Z, G_F) &= 79.8244\,\text{GeV}, \quad \Gamma_W = 2.085\,\text{GeV}, \\ m_h &= 125.0\,\text{GeV}, \qquad \Gamma_h = 4.07\,\text{MeV}. \end{aligned} \tag{4.1}$$

Notably, in this scheme the above value of m_W is not used as input but calculated from the input parameters by means of SM tree-level relations, which are not altered by any EFT contribution at the order we are considering. We use a diagonal CKM-matrix and exclude top quarks from the set of possible external states.

Scale uncertainties are included by means of a three-point scale variation of the renormalisation and factorisation scales, $\mu_R = \mu_F = \xi\mu_0$ with $\xi \in \{1/2, 1, 2\}$ and the central scale being chosen as in [12],

$$\mu_0 = \sqrt{\frac{m_h}{2}\sqrt{\frac{m_h^2}{4} + p_{\perp,hh}^2}}\,. \tag{4.2}$$

In [12] it is argued that this scale approximates well the square root of the product of the virtualities of the two vector bosons.

Jets are clustered with the anti-k_T algorithm [91] implemented in the FastJet package [92] with a radius parameter of $R = 0.4$. We require the presence of at least two jets satisfying

$$p_{\perp,j} > 20\,\text{GeV} \quad \text{and} \quad |y_j| < 4.5. \tag{4.3}$$

We apply some additional cuts on the invariant mass and pseudo-rapidity separation of the two hardest jets j_1 and j_2, referred to as *tagging jets*,

$$m_{j_1 j_2} > 600\,\text{GeV} \quad \text{and} \quad |\eta_{j_1} - \eta_{j_2}| > 4.0. \tag{4.4}$$

JHEP07(2025)209

No.	c_λ	c_V	c_{2V}	σ_{NLO} in fb	σ_{LO} in fb	$\sigma_{\text{NLO}}/\sigma_{\text{LO}}$	$\sigma_{\text{NLO}}/\sigma^{\text{SM}}_{\text{NLO}}$
SM	1.0	1.0	1.0	$0.752^{+0.000}_{-0.012} \pm 0.005$	$0.832^{+0.079}_{-0.074} \pm 0.002$	0.904(6)	1.00(1)
1	-1.0	0.9	1.5	$2.11^{+0.00}_{-0.07} \pm 0.01$	$2.321^{+0.297}_{-0.250} \pm 0.003$	0.910(4)	2.81(2)
2	-1.0	1.05	1.3	$3.40^{+0.03}_{-0.10} \pm 0.02$	$3.753^{+0.310}_{-0.286} \pm 0.007$	0.905(5)	4.51(4)
3	0.0	1.0	1.0	$1.94^{+0.01}_{-0.06} \pm 0.01$	$2.139^{+0.189}_{-0.173} \pm 0.004$	0.907(7)	2.58(3)
4	1.0	0.9	1.0	$0.380^{+0.000}_{-0.014} \pm 0.003$	$0.412^{+0.051}_{-0.038} \pm 0.002$	0.920(7)	0.505(5)
5	1.0	1.0	0.5	$4.38^{+0.03}_{-0.07} \pm 0.02$	$4.850^{+0.549}_{-0.445} \pm 0.007$	0.902(4)	5.82(5)
6	1.0	1.0	1.5	$1.52^{+0.00}_{-0.06} \pm 0.01$	$1.675^{+0.215}_{-0.177} \pm 0.002$	0.910(4)	2.03(2)
7	2.0	0.9	1.4	$3.86^{+0.02}_{-0.09} \pm 0.01$	$4.276^{+0.497}_{-0.402} \pm 0.004$	0.902(3)	5.13(4)
8	2.0	1.0	1.0	$0.627^{+0.000}_{-0.035} \pm 0.005$	$0.690^{+0.069}_{-0.063} \pm 0.002$	0.908(8)	0.833(8)
9	3.0	1.1	0.5	$4.40^{+0.00}_{-0.13} \pm 0.02$	$4.793^{+0.608}_{-0.488} \pm 0.006$	0.918(4)	5.85(5)
10	4.0	0.95	0.5	$2.41^{+0.01}_{-0.05} \pm 0.01$	$2.653^{+0.269}_{-0.227} \pm 0.005$	0.907(5)	3.12(3)
11	6.0	1.1	1.0	$9.82^{+0.00}_{-0.25} \pm 0.07$	$10.95^{+1.03}_{-0.74} \pm 0.02$	0.896(7)	13.1(1)

Table 1. LO and NLO cross sections at a centre-of-mass energy of $\sqrt{s} = 13.6\,\text{TeV}$ for various values of the anomalous couplings. The asymmetrical errors are calculated with a three-point scale variation, the symmetrical error is the MC integration error. For the ratios in the last two columns, only the MC error is given.

4.2 Total cross section

First, in table 1, we present the total cross sections at LO and at NLO for several selected benchmark points in (c_λ, c_V, c_{2V})-space. The ranges in which the anomalous couplings are varied are oriented at the constraints from refs. [1, 2]. Concretely, we use

$$c_\lambda \in [-1, 6]\ ,\ c_V \in [0.9, 1.1]\ ,\ c_{2V} \in [0.5, 1.5]\ . \tag{4.5}$$

We can immediately observe a significant dependence of the total cross section on the anomalous couplings, reaching an enhancement of more than an order of magnitude for benchmark point 11 or a decrease to less than half for benchmark point 4. In contrast to this, the K-factor depends only very mildly on the coupling values, varying by at most a few per cent. For the scale uncertainties, we can observe a clear reduction from LO to NLO.

To achieve a continuous description of the total cross section with respect to the anomalous couplings, we parametrise it as a polynomial in all possible combinations of anomalous couplings that can occur in the squared matrix element,

$$\frac{\sigma}{\sigma^{\text{SM}}} = A_0\ c_\lambda^2 c_V^2 + A_1\ c_V^4 + A_2\ c_{2V}^2 + A_3\ c_\lambda c_V^3 + A_4\ c_\lambda c_V c_{2V} + A_5\ c_V^2 c_{2V}. \tag{4.6}$$

Note that, since anomalous couplings only appear in the sub-diagrams shown in figure 1(b), the functional form of this parametrisation is the same at LO and NLO. We obtain values for the coefficients A_i by fitting the parametrisation (4.6) to the cross sections of the benchmark points in table 1 using the Python package `iminuit` [93, 94]. We repeat this procedure for $\mu_R = \mu_F = \mu_0/2$ and $\mu_R = \mu_F = 2\mu_0$, resulting in the coefficients shown in table 2.

This parametrisation can now be used to investigate the dependence of the total cross sections on the anomalous couplings in the considered parameter space. Figure 3 (left) shows

JHEP07(2025)209

Parameter	$\mu_F = \mu_r = \mu_0/2$	$\mu_F = \mu_r = \mu_0$	$\mu_F = \mu_r = 2\mu_0$
A_0	0.687(7)	0.693(5)	0.699(5)
A_1	21.8(2)	21.9(2)	22.0(2)
A_2	11.6(1)	11.7(1)	11.7(1)
A_3	−6.04(6)	−6.07(4)	−6.13(5)
A_4	3.80(4)	3.82(3)	3.86(3)
A_5	−30.9(3)	−31.0(2)	−31.2(2)

Table 2. Fit results for the coefficients of equation (4.6) with the central scale given by equation (4.2). The uncertainties are those obtained in the fitting procedure.

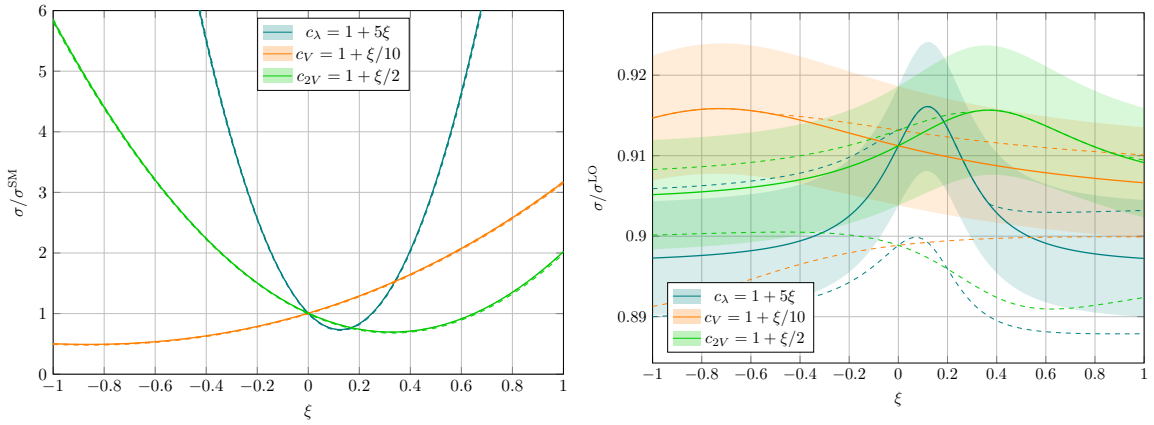

Figure 3. Ratio of the total cross section to the SM cross section at NLO (left) and to the LO cross section (right) for variations of a single coupling. The bands show the uncertainties resulting from the uncertainties of the fit coefficients, the dashed lines show the change due to the scale variation.

the dependence of the cross section on a single anomalous coupling, where all other couplings are kept at the SM value. The impact of the different parameters varies strongly, with c_λ having the largest impact, while c_V has the smallest impact. However, this is mostly a result of the size of the respective parameter ranges. The vector boson couplings are much tighter constrained than the triple-Higgs coupling, allowing the latter to deviate much more from the SM value. Nonetheless, all couplings can significantly alter the cross section. Maximising the function over the allowed parameter range leads to a value of about 27 times the SM cross section.[5]

The right-hand side of figure 3 shows the ratio of the total NLO cross section to the respective LO value, σ_{NLO}/σ_{LO}. We see that varying a single parameter over its whole parameter space impacts the ratio by less than 3%. We can also observe the impact of the scale variation to be only relatively small, with the uncertainty due to the scale variation being of similar size as the uncertainties from the fit.

So far, only variations of a single coupling were considered. In figure 4, the simultaneous variation of two couplings is depicted. The left column contains the total NLO cross section

[5]To the best of our knowledge, the currently best experimental bound on the total cross section is 44 times the SM cross section [95].

JHEP07(2025)209

relative to the SM, the right column again contains the ratio to the LO cross section, $\sigma_{\mathrm{NLO}}/\sigma_{\mathrm{LO}}$. For the slices shown in the coupling parameter space, the third (not shown) coupling is set to its SM value. Variations in the ratio to LO still do not exceed the 3% range, in agreement with the observations above. However, the left column shows that there is a quite strong dependence of the total cross section on the values of the anomalous couplings. For large values of c_λ and c_{2V}, the cross section can exceed the SM cross section by a factor of about 20, while for small values of c_V, the cross section can decrease.

4.3 Differential distributions

Finally, we show differential results for four different observables: the transverse momentum distribution $p_\perp^h$ of the Higgs bosons, the Higgs boson pair invariant mass m_{hh}, the pseudo-rapidity separation between the Higgs bosons, $\Delta\eta(h,h)$, and the R-separation between the Higgs bosons, $\Delta R(h,h) = \sqrt{\Delta\phi^2 + \Delta\eta^2}$. As the K-factor due to the NLO QCD corrections is mostly flat, we refrain from showing the SM LO and NLO curves and instead focus on the effects of the anomalous couplings on the NLO QCD results. In particular, we show those benchmark points where a certain *combination* of anomalous couplings has a more pronounced effect on the shape of the distribution than varying any of these couplings individually.

In figure 5 we show the $p_\perp^h$ distribution for benchmark points 1, 4, 6 and 8 (left) and the m_{hh} distribution for benchmark points 1, 3, 4, and 6 (right). The $p_\perp^h$ distribution clearly exhibits that variations of c_λ alone do not have a dramatic effect, while changes in c_V and c_{2V} affect the delicate cancellations in the SM that guarantee unitarity and therefore have a large effect at high $p_\perp^h$. Unitarity constraints for the process $VV \to hh$ have been discussed in detail in ref. [23]. Purely theoretical constraints can be useful to complement experimental constraints, see e.g. [96, 97] for recent studies.This subject is beyond the scope of this paper, however.

The invariant mass of the di-Higgs system can show dramatic shape changes compared to the SM, both at low and high m_{hh}-values, where the changes at low m_{hh} are induced by c_λ being different from the SM value. For benchmark point 1, destructive interference between different contributions leads to a characteristic peak-dip structure. It is interesting to note that such a peak-dip structure is not present if c_λ is only varied individually.

We observed the largest shape changes in the $\Delta\eta(h,h)$ distribution, shown in figure 6 (left), as well as some interesting features in the $\Delta R(h,h)$ distribution (figure 6 right). The former distribution is shown for the benchmark points 4, 5 and 10, the latter for 4, 6 and 10. In the SM, most Higgs boson pairs are produced with a pseudorapidity separation of about 2.5 and a clear local minimum at $\Delta\eta(h,h) = 0$. However, this dip becomes a local maximum for the shown benchmark points, for example forming a distinct peak for benchmark point 10, which is $(c_\lambda, c_V, c_{2V}) = (4, 0.95, 0.5)$. This behaviour can be understood by considering the diagrams in figure 1(b). The contribution of the leftmost diagram is enhanced for large self-couplings, leading to an excess in less well separated Higgs bosons, since they originate from the same triple Higgs three-point vertex.

The changes in the pseudo-rapidity separation also influence the R-separation ΔR of the Higgs bosons. This distribution is also skewed towards smaller ΔR values for large values of c_λ, due to the dominance of the contribution from diagrams with an s-channel Higgs

JHEP07(2025)209

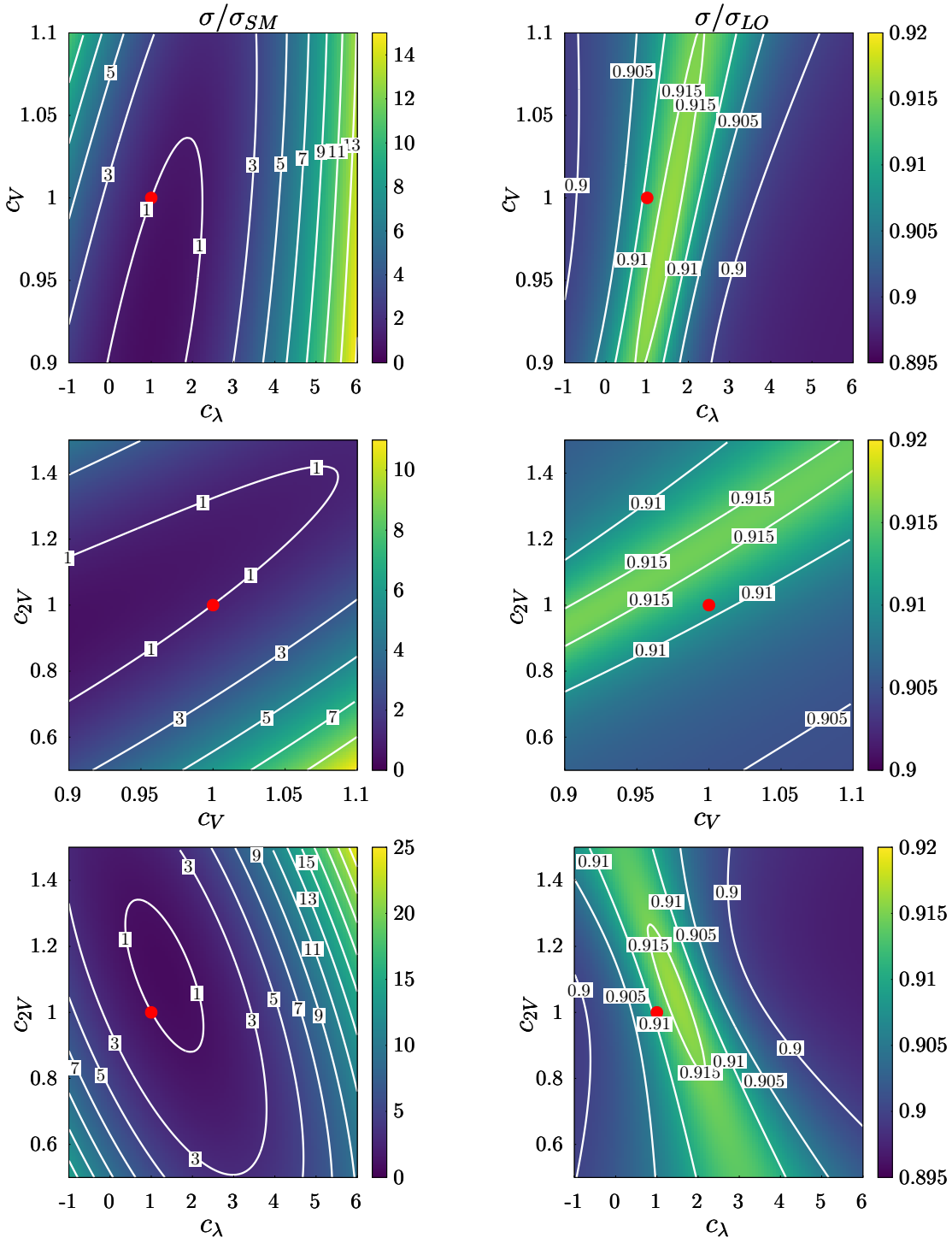

Figure 4. Ratio of the total cross section to the SM cross section at NLO (left column) and to the LO cross section (right column) in the c_λ-c_V plane (first row), c_V-c_{2V} plane (second row) and c_λ-c_{2V} plane (third row). The red dot indicates the SM coupling values.

JHEP07(2025)209

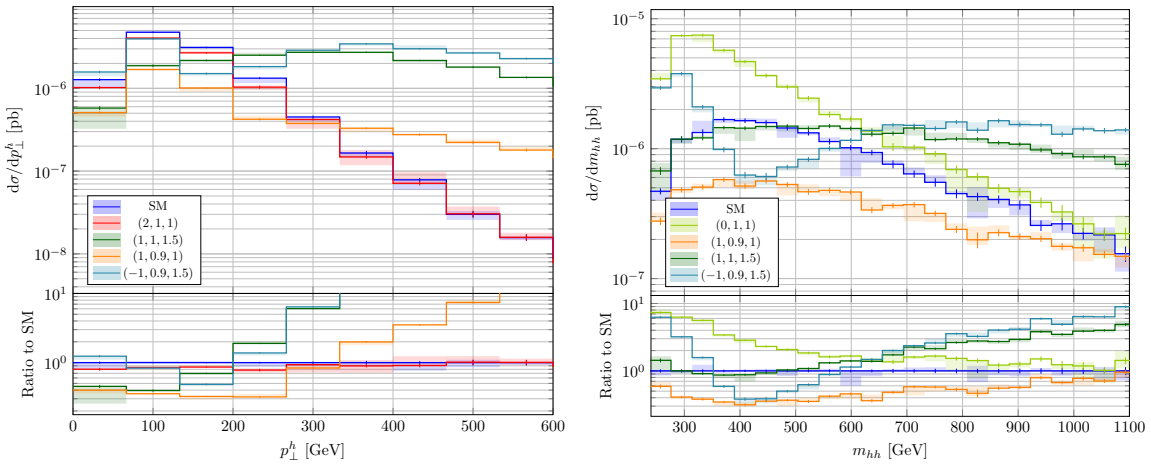

Figure 5. Transverse momentum distribution of (any of) the Higgs bosons (left) and invariant-mass distribution of the di-Higgs system (right) for selected benchmark points in (c_λ, c_V, c_{2V})-space of table 1 at NLO.

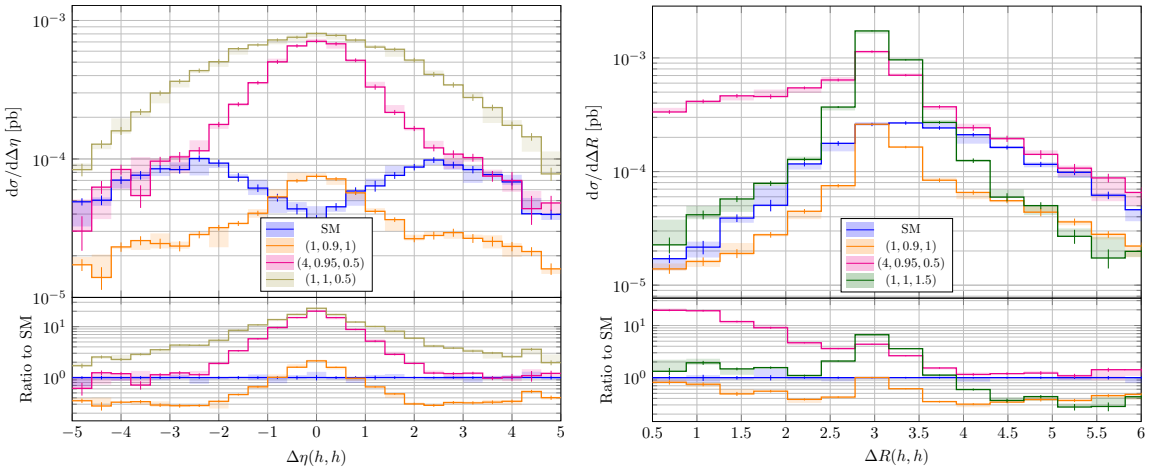

Figure 6. Pseudorapidity separation distribution (left) and ΔR-separation distribution (right) of the Higgs pair for selected benchmark points in (c_λ, c_V, c_{2V})-space (see table 1) at NLO.

propagator. However, due to a simultaneous increase in $\Delta\phi$ for anomalous values of the Higgs-vector boson couplings, another interesting feature can be observed: increasing the Higgs boson self-coupling only increases the abundance of low ΔR events, while for variations of the other two couplings, a peak develops around $\Delta R \sim \pi$. The large-ΔR region is much less affected by changes in the couplings.

JHEP07(2025)209

5 Conclusions

We have calculated the NLO QCD corrections to Higgs boson pair production in vector boson fusion and included the leading anomalous couplings within non-linear Effective Field Theory (HEFT). We explained in detail the derivation of the HEFT Lagrangian for this process and the contributing diagrams. We did not use the structure function approximation; diagrams of u- and s-channel type ("Higgs-Strahlung topologies") are also included.

Our results are based on an automated Whizard-GoSam interface that can be used for user-defined NLO calculations for both hadronic or leptonic collisions, including the option to use UFO model files and flexible setups for calculations beyond the SM. The new releases of both tools are close to completion. This setup also allows for parton showering, however we did not add a shower in the present work.

As is well known, the NLO QCD corrections in the SM reduce the cross section by about 7% with a relatively flat K-factor. The K-factors relative to the SM K-factors also do not vary by more then about 3% when introducing anomalous couplings, which can be understood from the fact that the QCD corrections of "structure function type" are dominating, while the anomalous couplings affect the electroweak part of the amplitude. We have parametrised the total cross section as a polynomial in the anomalous couplings and fitted the coefficients based on our NLO calculation. This offers a flexible representation of the cross section that allows fast evaluation for arbitrary values of the couplings. Based on this parametrisation, we have shown heat maps for slices of the (c_λ, c_V, c_{2V})-parameter space illustrating the ratio to the SM cross section and the respective LO cross section.

In the anomalous coupling parameter space, we defined 11 benchmark points, oriented at the current experimental constraints, which lead to characteristic shapes in the $p_\perp^h$, m_{hh}, $\Delta\eta(h,h)$ or $\Delta R(h,h)$ distributions. It is not surprising that modifications of c_V or c_{2V} can have large effects in the high-energy tails of the distributions, as the SM-type unitarity cancellations are spoiled and may only set in later through a particular UV completion. A feature that is noteworthy is the fact that combinations of anomalous couplings can lead to characteristic shapes that would not occur if any of the couplings was varied in isolation. This feature also can be observed in phase space regions that are experimentally more accessible than the tails of distributions, such as the central region of the pseudo-rapidity difference $\Delta\eta(h,h)$. Such characteristic shapes could signpost physics beyond the SM even with moderate experimental statistics.

Note added. During completion of this paper, we became aware of similar work [98], where an NLO+PS calculation of this process is presented in the `Powheg-Box-V2` framework, also accounting for anomalous couplings, together with an upgrade of the program `proVBFHH` [16]. However, the two calculations are in large parts complementary: the work of [98] focuses on the comparison between the NNLO results and the NLO+PS results and uses the structure function approximation. Our calculation does not use this approximation and focuses on the derivation of the leading operators in HEFT and how the corresponding anomalous couplings affect the shape of distributions if varied simultaneously. We leave a more detailed comparison for future work.

JHEP07(2025)209

Acknowledgments

We would like to thank Alexander Karlberg, Barbara Jäger and Simon Reinhardt for sharing their draft with us before publication. We also would like to thank Jannis Lang for work on the EFT aspects of GoSam and Jürgen Reuter and Wolfgang Kilian for input concerning the Whizard-GoSam interface. This research was supported by the Deutsche Forschungsgemeinschaft (DFG, German Research Foundation) under grant 396021762 — TRR 257. The authors also acknowledge support by the state of Baden-Württemberg through bwHPC.

Data Availability Statement. This article has no associated data or the data will not be deposited.

Code Availability Statement. This article has no associated code or the code will not be deposited.

References

[1] ATLAS collaboration, *Combination of searches for Higgs boson pair production in pp collisions at $\sqrt{s} = 13$ TeV with the ATLAS detector*, *Phys. Rev. Lett.* **133** (2024) 101801 [arXiv:2406.09971] [INSPIRE].

[2] CMS collaboration, *Constraints on the Higgs boson self-coupling from the combination of single and double Higgs boson production in proton-proton collisions at $\sqrt{s} = 13$ TeV*, *Phys. Lett. B* **861** (2025) 139210 [arXiv:2407.13554] [INSPIRE].

[3] ATLAS collaboration, *Search for pair production of boosted Higgs bosons via vector-boson fusion in the $b\bar{b}b\bar{b}$ final state using pp collisions at $\sqrt{s} = 13$ TeV with the ATLAS detector*, *Phys. Lett. B* **858** (2024) 139007 [arXiv:2404.17193] [INSPIRE].

[4] CMS collaboration, *Combination of searches for nonresonant Higgs boson pair production in proton-proton collisions at $\sqrt{s} = 13$ TeV*, CMS-PAS-HIG-20-011, CERN, Geneva, Switzerland (2024) [INSPIRE].

[5] T. Figy, *Next-to-leading order QCD corrections to light Higgs pair production via vector boson fusion*, *Mod. Phys. Lett. A* **23** (2008) 1961 [arXiv:0806.2200] [INSPIRE].

[6] J. Baglio et al., *The measurement of the Higgs self-coupling at the LHC: theoretical status*, *JHEP* **04** (2013) 151 [arXiv:1212.5581] [INSPIRE].

[7] R. Frederix et al., *Higgs pair production at the LHC with NLO and parton-shower effects*, *Phys. Lett. B* **732** (2014) 142 [arXiv:1401.7340] [INSPIRE].

[8] K. Arnold et al., *VBFNLO: a parton level Monte Carlo for processes with electroweak bosons*, *Comput. Phys. Commun.* **180** (2009) 1661 [arXiv:0811.4559] [INSPIRE].

[9] J. Baglio et al., *Release note: VBFNLO 3.0*, *Eur. Phys. J. C* **84** (2024) 1003 [arXiv:2405.06990] [INSPIRE].

JHEP07(2025)209

[10] J. Alwall et al., *The automated computation of tree-level and next-to-leading order differential cross sections, and their matching to parton shower simulations*, *JHEP* **07** (2014) 079 [arXiv:1405.0301] [INSPIRE].

[11] L.-S. Ling et al., *NNLO QCD corrections to Higgs pair production via vector boson fusion at hadron colliders*, *Phys. Rev. D* **89** (2014) 073001 [arXiv:1401.7754] [INSPIRE].

[12] F.A. Dreyer and A. Karlberg, *Fully differential vector-boson fusion Higgs pair production at next-to-next-to-leading order*, *Phys. Rev. D* **99** (2019) 074028 [arXiv:1811.07918] [INSPIRE].

[13] F.A. Dreyer and A. Karlberg, *Vector-boson fusion Higgs pair production at N^3LO*, *Phys. Rev. D* **98** (2018) 114016 [arXiv:1811.07906] [INSPIRE].

[14] F.A. Dreyer, A. Karlberg, J.-N. Lang and M. Pellen, *Precise predictions for double-Higgs production via vector-boson fusion*, *Eur. Phys. J. C* **80** (2020) 1037 [arXiv:2005.13341] [INSPIRE].

[15] F.A. Dreyer, A. Karlberg and L. Tancredi, *On the impact of non-factorisable corrections in VBF single and double Higgs production*, *JHEP* **10** (2020) 131 [*Erratum ibid.* **04** (2022) 009] [arXiv:2005.11334] [INSPIRE].

[16] A. Karlberg, *proVBFHH*, https://github.com/alexanderkarlberg/proVBFH.

[17] M.J. Dolan, C. Englert, N. Greiner and M. Spannowsky, *Further on up the road: $hhjj$ production at the LHC*, *Phys. Rev. Lett.* **112** (2014) 101802 [arXiv:1310.1084] [INSPIRE].

[18] M.J. Dolan et al., *$hhjj$ production at the LHC*, *Eur. Phys. J. C* **75** (2015) 387 [arXiv:1506.08008] [INSPIRE].

[19] F. Bishara, R. Contino and J. Rojo, *Higgs pair production in vector-boson fusion at the LHC and beyond*, *Eur. Phys. J. C* **77** (2017) 481 [arXiv:1611.03860] [INSPIRE].

[20] L.-S. Ling et al., *Dimension-six operators in Higgs boson pair production via vector-boson fusion at the LHC*, *Phys. Rev. D* **96** (2017) 055006 [arXiv:1708.04785] [INSPIRE].

[21] E. Arganda, C. Garcia-Garcia and M.J. Herrero, *Probing the Higgs self-coupling through double Higgs production in vector boson scattering at the LHC*, *Nucl. Phys. B* **945** (2019) 114687 [arXiv:1807.09736] [INSPIRE].

[22] J.Y. Araz, S. Banerjee, R.S. Gupta and M. Spannowsky, *Precision SMEFT bounds from the VBF Higgs at high transverse momentum*, *JHEP* **04** (2021) 125 [arXiv:2011.03555] [INSPIRE].

[23] W. Kilian et al., *Multi-Higgs boson production and unitarity in vector-boson fusion at future hadron colliders*, *Phys. Rev. D* **101** (2020) 076012 [arXiv:1808.05534] [INSPIRE].

[24] W. Kilian et al., *Highly boosted Higgs bosons and unitarity in vector-boson fusion at future hadron colliders*, *JHEP* **05** (2021) 198 [arXiv:2101.12537] [INSPIRE].

[25] R. Gómez-Ambrosio, F.J. Llanes-Estrada, A. Salas-Bernárdez and J.J. Sanz-Cillero, *Distinguishing electroweak EFTs with $W_LW_L \to n\,h$*, *Phys. Rev. D* **106** (2022) 053004 [arXiv:2204.01763] [INSPIRE].

[26] R. Gómez-Ambrosio, F.J. Llanes-Estrada, A. Salas-Bernárdez and J.J. Sanz-Cillero, *SMEFT is falsifiable through multi-Higgs measurements (even in the absence of new light particles)*, *Commun. Theor. Phys.* **75** (2023) 095202 [arXiv:2207.09848] [INSPIRE].

[27] M.J. Herrero and R.A. Morales, *One-loop corrections for $WW \to HH$ in Higgs EFT with the electroweak chiral Lagrangian*, *Phys. Rev. D* **106** (2022) 073008 [arXiv:2208.05900] [INSPIRE].

[28] Anisha et al., *Bosonic multi-Higgs correlations beyond leading order*, *Phys. Rev. D* **110** (2024) 095016 [arXiv:2405.05385] [INSPIRE].

JHEP07(2025)209

[29] Anisha et al., *HEFT's appraisal of triple (versus double) Higgs weak boson fusion*, *Phys. Rev. D* **111** (2025) 055004 [arXiv:2407.20706] [INSPIRE].

[30] F. Feruglio, *The chiral approach to the electroweak interactions*, *Int. J. Mod. Phys. A* **8** (1993) 4937 [hep-ph/9301281] [INSPIRE].

[31] J. Bagger et al., *The strongly interacting WW system: gold plated modes*, *Phys. Rev. D* **49** (1994) 1246 [hep-ph/9306256] [INSPIRE].

[32] V. Koulovassilopoulos and R.S. Chivukula, *The phenomenology of a nonstandard Higgs boson in W_LW_L scattering*, *Phys. Rev. D* **50** (1994) 3218 [hep-ph/9312317] [INSPIRE].

[33] C.P. Burgess, J. Matias and M. Pospelov, *A Higgs or not a Higgs? What to do if you discover a new scalar particle*, *Int. J. Mod. Phys. A* **17** (2002) 1841 [hep-ph/9912459] [INSPIRE].

[34] L.-M. Wang and Q. Wang, *Nonstandard Higgs in electroweak chiral Lagrangian*, hep-ph/0605104 [INSPIRE].

[35] B. Grinstein and M. Trott, *A Higgs-Higgs bound state due to new physics at a TeV*, *Phys. Rev. D* **76** (2007) 073002 [arXiv:0704.1505] [INSPIRE].

[36] R. Alonso et al., *The effective chiral Lagrangian for a light dynamical "Higgs particle"*, *Phys. Lett. B* **722** (2013) 330 [*Erratum ibid.* **726** (2013) 926] [arXiv:1212.3305] [INSPIRE].

[37] G. Buchalla and O. Cata, *Effective theory of a dynamically broken electroweak Standard Model at NLO*, *JHEP* **07** (2012) 101 [arXiv:1203.6510] [INSPIRE].

[38] G. Buchalla, O. Catà and C. Krause, *Complete electroweak chiral Lagrangian with a light Higgs at NLO*, *Nucl. Phys. B* **880** (2014) 552 [arXiv:1307.5017] [INSPIRE].

[39] C. Degrande et al., *Automated one-loop computations in the Standard Model Effective Field Theory*, *Phys. Rev. D* **103** (2021) 096024 [arXiv:2008.11743] [INSPIRE].

[40] GoSam collaboration, *Automated one-loop calculations with GoSam*, *Eur. Phys. J. C* **72** (2012) 1889 [arXiv:1111.2034] [INSPIRE].

[41] GoSam collaboration, *GoSam-2.0: a tool for automated one-loop calculations within the Standard Model and beyond*, *Eur. Phys. J. C* **74** (2014) 3001 [arXiv:1404.7096] [INSPIRE].

[42] J. Braun et al., *GoSam-3.0*, to appear.

[43] M. Moretti, T. Ohl and J. Reuter, *O'Mega: an optimizing matrix element generator*, hep-ph/0102195 [INSPIRE].

[44] W. Kilian, T. Ohl and J. Reuter, *WHIZARD: simulating multi-particle processes at LHC and ILC*, *Eur. Phys. J. C* **71** (2011) 1742 [arXiv:0708.4233] [INSPIRE].

[45] T. Binoth et al., *A proposal for a standard interface between Monte Carlo tools and one-loop programs*, *Comput. Phys. Commun.* **181** (2010) 1612 [arXiv:1001.1307] [INSPIRE].

[46] S. Alioli et al., *Update of the Binoth Les Houches accord for a standard interface between Monte Carlo tools and one-loop programs*, *Comput. Phys. Commun.* **185** (2014) 560 [arXiv:1308.3462] [INSPIRE].

[47] C. Degrande et al., *UFO — the Universal FeynRules Output*, *Comput. Phys. Commun.* **183** (2012) 1201 [arXiv:1108.2040] [INSPIRE].

[48] L. Darmé et al., *UFO 2.0: the "Universal Feynman Output" format*, *Eur. Phys. J. C* **83** (2023) 631 [arXiv:2304.09883] [INSPIRE].

[49] W. Buchmüller and D. Wyler, *Effective Lagrangian analysis of new interactions and flavor conservation*, *Nucl. Phys. B* **268** (1986) 621 [INSPIRE].

JHEP07(2025)209

[50] B. Grzadkowski, M. Iskrzynski, M. Misiak and J. Rosiek, *Dimension-six terms in the Standard Model Lagrangian*, *JHEP* **10** (2010) 085 [arXiv:1008.4884] [INSPIRE].

[51] I. Brivio and M. Trott, *The Standard Model as an Effective Field Theory*, *Phys. Rept.* **793** (2019) 1 [arXiv:1706.08945] [INSPIRE].

[52] G. Isidori, F. Wilsch and D. Wyler, *The Standard Model Effective Field Theory at work*, *Rev. Mod. Phys.* **96** (2024) 015006 [arXiv:2303.16922] [INSPIRE].

[53] C. Arzt, M.B. Einhorn and J. Wudka, *Patterns of deviation from the Standard Model*, *Nucl. Phys. B* **433** (1995) 41 [hep-ph/9405214] [INSPIRE].

[54] N. Craig, M. Jiang, Y.-Y. Li and D. Sutherland, *Loops and trees in generic EFTs*, *JHEP* **08** (2020) 086 [arXiv:2001.00017] [INSPIRE].

[55] G. Buchalla, G. Heinrich, C. Müller-Salditt and F. Pandler, *Loop counting matters in SMEFT*, *SciPost Phys.* **15** (2023) 088 [arXiv:2204.11808] [INSPIRE].

[56] G. Buchalla, O. Catá and C. Krause, *On the power counting in Effective Field Theories*, *Phys. Lett. B* **731** (2014) 80 [arXiv:1312.5624] [INSPIRE].

[57] H. Sun, M.-L. Xiao and J.-H. Yu, *Complete NLO operators in the Higgs Effective Field Theory*, *JHEP* **05** (2023) 043 [arXiv:2206.07722] [INSPIRE].

[58] L. Gráf et al., *Hilbert series, the Higgs mechanism, and HEFT*, *JHEP* **02** (2023) 064 [arXiv:2211.06275] [INSPIRE].

[59] R. Alonso, K. Kanshin and S. Saa, *Renormalization group evolution of Higgs Effective Field Theory*, *Phys. Rev. D* **97** (2018) 035010 [arXiv:1710.06848] [INSPIRE].

[60] G. Buchalla et al., *Complete one-loop renormalization of the Higgs-electroweak chiral Lagrangian*, *Nucl. Phys. B* **928** (2018) 93 [arXiv:1710.06412] [INSPIRE].

[61] G. Buchalla et al., *Higgs-electroweak chiral Lagrangian: one-loop renormalization group equations*, *Phys. Rev. D* **104** (2021) 076005 [arXiv:2004.11348] [INSPIRE].

[62] M.E. Peskin and T. Takeuchi, *Estimation of oblique electroweak corrections*, *Phys. Rev. D* **46** (1992) 381 [INSPIRE].

[63] J. de Blas et al., *Global analysis of electroweak data in the Standard Model*, *Phys. Rev. D* **106** (2022) 033003 [arXiv:2112.07274] [INSPIRE].

[64] LHC Higgs Cross Section Working Group collaboration, *LHC HXSWG interim recommendations to explore the coupling structure of a Higgs-like particle*, arXiv:1209.0040 [INSPIRE].

[65] LHC Higgs Cross Section Working Group collaboration, *Handbook of LHC Higgs cross sections: 3. Higgs properties*, arXiv:1307.1347 [DOI:10.5170/CERN-2013-004] [INSPIRE].

[66] J. de Blas, O. Eberhardt and C. Krause, *Current and future constraints on Higgs couplings in the nonlinear effective theory*, *JHEP* **07** (2018) 048 [arXiv:1803.00939] [INSPIRE].

[67] M. Ciccolini, A. Denner and S. Dittmaier, *Electroweak and QCD corrections to Higgs production via vector-boson fusion at the LHC*, *Phys. Rev. D* **77** (2008) 013002 [arXiv:0710.4749] [INSPIRE].

[68] C. Bierlich et al., *Robust independent validation of experiment and theory: Rivet version 3*, *SciPost Phys.* **8** (2020) 026 [arXiv:1912.05451] [INSPIRE].

[69] C. Bierlich et al., *Robust independent validation of experiment and theory: Rivet version 4 release note*, *SciPost Phys. Codeb.* **36** (2024) 1 [arXiv:2404.15984] [INSPIRE].

JHEP07(2025)209

[70] T. Ohl, *Vegas revisited: adaptive Monte Carlo integration beyond factorization*, *Comput. Phys. Commun.* **120** (1999) 13 [hep-ph/9806432] [INSPIRE].

[71] S. Brass, W. Kilian and J. Reuter, *Parallel adaptive Monte Carlo integration with the event generator WHIZARD*, *Eur. Phys. J. C* **79** (2019) 344 [arXiv:1811.09711] [INSPIRE].

[72] B. Chokoufé Nejad et al., *NLO QCD predictions for off-shell $t\bar{t}$ and $t\bar{t}H$ production and decay at a linear collider*, *JHEP* **12** (2016) 075 [arXiv:1609.03390] [INSPIRE].

[73] P. Stienemeier et al., *WHIZARD 3.0: status and news*, in the proceedings of the *International Workshop on Future Linear Colliders*, (2021) [arXiv:2104.11141] [INSPIRE].

[74] S. Frixione, Z. Kunszt and A. Signer, *Three jet cross-sections to next-to-leading order*, *Nucl. Phys. B* **467** (1996) 399 [hep-ph/9512328] [INSPIRE].

[75] S. Frixione, *A general approach to jet cross-sections in QCD*, *Nucl. Phys. B* **507** (1997) 295 [hep-ph/9706545] [INSPIRE].

[76] P. Nason, *A new method for combining NLO QCD with shower Monte Carlo algorithms*, *JHEP* **11** (2004) 040 [hep-ph/0409146] [INSPIRE].

[77] P. Stienemeier, *Automation and application of fixed-order and matched NLO simulations*, Ph.D. thesis, Hamburg U., Hamburg, Germany (2022) [INSPIRE].

[78] P. Nogueira, *Automatic Feynman graph generation*, *J. Comput. Phys.* **105** (1993) 279 [INSPIRE].

[79] J.A.M. Vermaseren, *New features of FORM*, math-ph/0010025 [INSPIRE].

[80] J. Kuipers, T. Ueda, J.A.M. Vermaseren and J. Vollinga, *FORM version 4.0*, *Comput. Phys. Commun.* **184** (2013) 1453 [arXiv:1203.6543] [INSPIRE].

[81] H. van Deurzen et al., *Multi-leg one-loop massive amplitudes from integrand reduction via Laurent expansion*, *JHEP* **03** (2014) 115 [arXiv:1312.6678] [INSPIRE].

[82] T. Peraro, *Ninja: automated integrand reduction via Laurent expansion for one-loop amplitudes*, *Comput. Phys. Commun.* **185** (2014) 2771 [arXiv:1403.1229] [INSPIRE].

[83] A. van Hameren, *OneLOop: for the evaluation of one-loop scalar functions*, *Comput. Phys. Commun.* **182** (2011) 2427 [arXiv:1007.4716] [INSPIRE].

[84] F. Maltoni, E. Vryonidou and C. Zhang, *Higgs production in association with a top-antitop pair in the Standard Model Effective Field Theory at NLO in QCD*, *JHEP* **10** (2016) 123 [arXiv:1607.05330] [INSPIRE].

[85] M. Van Geest, *Anomalous couplings within Standard Model Effective Field Theory in ttH production at NLO QCD*, Master thesis, Karlsruhe Institute of Technology, Karlsruhe, Germany (2024) [INSPIRE].

[86] F. Cascioli, P. Maierhofer and S. Pozzorini, *Scattering amplitudes with OpenLoops*, *Phys. Rev. Lett.* **108** (2012) 111601 [arXiv:1111.5206] [INSPIRE].

[87] F. Buccioni et al., *OpenLoops 2*, *Eur. Phys. J. C* **79** (2019) 866 [arXiv:1907.13071] [INSPIRE].

[88] J. Braun, *Higgs boson pair production in vector boson fusion at NLO QCD in HEFT*, Master thesis, Karlsruhe Institute of Technology, Karlsruhe, Germany (2024).

[89] PDF4LHC Working Group collaboration, *The PDF4LHC21 combination of global PDF fits for the LHC run III*, *J. Phys. G* **49** (2022) 080501 [arXiv:2203.05506] [INSPIRE].

[90] A. Buckley et al., *LHAPDF6: parton density access in the LHC precision era*, *Eur. Phys. J. C* **75** (2015) 132 [arXiv:1412.7420] [INSPIRE].

JHEP07(2025)209

[91] M. Cacciari, G.P. Salam and G. Soyez, *The anti-k_t jet clustering algorithm*, *JHEP* **04** (2008) 063 [arXiv:0802.1189] [INSPIRE].

[92] M. Cacciari, G.P. Salam and G. Soyez, *FastJet user manual*, *Eur. Phys. J. C* **72** (2012) 1896 [arXiv:1111.6097] [INSPIRE].

[93] H. Dembinski et al., *scikit-hep/iminuit*, https://github.com/scikit-hep/iminuit.

[94] F. James and M. Roos, *Minuit: a system for function minimization and analysis of the parameter errors and correlations*, *Comput. Phys. Commun.* **10** (1975) 343 [INSPIRE].

[95] A.R. Martinez„ *Overview of HH searches at ATLAS*, talk at the *21st workshop of the LHC Higgs working group*, https://indico.cern.ch/event/1389221/contributions/6195709/ (2024).

[96] T. Cohen, N. Craig, X. Lu and D. Sutherland, *Unitarity violation and the geometry of Higgs EFTs*, *JHEP* **12** (2021) 003 [arXiv:2108.03240] [INSPIRE].

[97] D. Barducci, M. Nardecchia and C. Toni, *Perturbative unitarity constraints on generic vector interactions*, *JHEP* **09** (2023) 134 [arXiv:2306.11533] [INSPIRE].

[98] B. Jäger, A. Karlberg and S. Reinhardt, *Precision tools for the simulation of double-Higgs production via vector-boson fusion*, *JHEP* **06** (2025) 022 [arXiv:2502.09112] [INSPIRE].

JHEP07(2025)209